Size-Dependent Structural and Magnetic Properties of Chemically Synthesized Co-Ni-Ga Nanoparticles

Changhai Wang [§], Aleksandr A. Levin[§], Julie Karel[§], Simone Fabbrici [#†], Jinfeng Qian[§], Carlos E. ViolBarbosa[§], Siham Ouardi[§], Franca Albertini[#], Walter Schnelle[§], Jan Rohlicek[§], Gerhard H. Fecher[§], and Claudia Felser[§]**

[§]Max Planck Institute for Chemical Physics of Solids, D-01187 Dresden, Germany

[#]Institute of Materials for Electronics and Magnetism, IMEM-CNR, I-43124 Parma, Italy

[†]MIST E-R Laboratory, Via Gobetti 101, I-40129 Bologna, Italy

* Corresponding author, E-mail: wngchai@gmail.com; Claudia.Felser@cpfs.mpg.de

Abstract

Phase transitions and magnetic properties of shape-memory materials can be tailored by tuning the size of the materials'constituent as nanoparticles. However, with the lack of a suitable synthesis method for size-controlled Heusler nanoparticles, there is no report on the size dependence of these properties and functionalities. In this contribution we present the first report on the chemical synthesis of size-selected Co-Ni-Ga Heusler nanoparticles. We report the structure and magnetic properties of the two-phase Co-Ni-Ga nanoparticles with sizes in the range of 30–84 nm, prepared by a SBA-15 assisted approach. The particle size can be readily tuned by controlling the loading method and concentration of the precursor. The fractions and crystallite sizes of each phase of the Co-Ni-Ga nanoparticles are closely related to their particle size. Enhanced magnetization and decreased coercivity are observed with increasing particle size. The Curie temperature (T_c) of the Co-Ni-Ga nanoparticles also depends on their size. The 84 nm particles exhibit the highest T_c (≈1174 K) among all known Heusler compounds. The Co-Ni-Ga nanoparticles exhibit very high Curie temperatures, which make them promising candidates for application in high-temperature shape memory alloy-based devices.

Key-words: Co-Ni-Ga, nanoparticles, chemical synthesis, size, magnetic properties

Introduction

Nanoscale shape memory materials have attracted increased interest with the recent trend of downsizing in shape-memory-effect-based functional devices [1-5]. Metallurgical methods such as re-crystallization from amorphous solid solutions have been widely used to obtain shape memory nanophases [6-10]. These nanophases, which formed in a wide distribution of sizes (typically up to hundreds of nanometers), were typically embedded in the parent phases. Other synthetic approaches were also developed for preparing shape memory nanoparticles, such as laser-induced pyrolysis [11], ball milling [12, 13], and vapor deposition [14], however, size control remained challenging. In a recent work, we introduced a new synthetic approach to prepare Co_2FeGa nanowires and nanoparticles using the two-dimensionally ordered SBA-15 mesoporous silica as templates [15]. Ongoing studies mostly focused on fabricating a variety of nanoparticles and nanowires within the pore channels of SBA-15 [16-19]. The numerous easily accessible surfaces of SBA-15 were, however, generally overlooked. The present work demonstrates the use of the outer surfaces of SBA-15 as templates for preparing Co-Ni-Ga shape memory Heusler nanoparticles with selected sizes in a range of 30–84 nm.

Ni-Mn-Ga nanoparticles were the first reported shape memory Heusler nanoparticles [12, 13]. They were prepared by a top-down ball-milling method from bulk alloys, which underwent a martensitic phase transformation. In applications, Ni-Mn-Ga Heusler alloys are unfavorable because of their low structural and magnetic transition temperatures and poor processability. Recently, Co-Ni-Ga Heusler compounds were thoroughly studied as potential alternatives to Ni-Mn-Ga, especially for high-temperature shape memory device applications [20, 21]. Co_2NiGa Heusler compounds frequently have a dual-phase structure: the main austenite phase (β) and the secondary tetragonal phase (γ). The B2-structured β-phase is typically Ni-deficient; a martensitic transformation occurs between the austenitic B2 and the tetragonal $L1_0$ martensite. The presence of the γ-phase significantly enhances the ductility of the Co-Ni-Ga alloys. The martensitic transformation and Curie temperatures were reported over wide distributions of 123–590 K and 360–950 K, respectively, for the bulk Co-Ni-Ga samples [20, 22-24]. These discrepancies in these

characteristic temperatures were attributed to differences in the preparation methods, compositions, crystal structures, and thermal treatments of the studied samples. Recently, we reported the structure and magnetic properties of Co_2NiGa nanoparticles of a single γ-phase (γ-Co_2NiGa) which exhibit a very high Curie temperature (≈ 1139 K) [25].

1. Experimental

1.1 Chemicals and synthesis

All chemicals were purchased from Sigma-Aldrich or Alfa Aesar and used as-received. The nonionic triblock copolymer, Pluronic P123 (MW 5800), and tetraethoxysilane (TEOS) were used as a structure-directing surfactant and a silicon source, respectively. Furthermore, the precursors for the Co-Ni-Ga nanoparticles were $CoCl_2 \cdot 6H_2O$ (99.9%), $Ni(NO_3)_2 \cdot 6H_2O$ (99.999%), and $Ga(NO_3)_3 \cdot xH_2O$ (99.9%).

Mesoporous SBA-15 silica was prepared following the procedures reported in the literature [26]. A successful preparation of Co-Ni-Ga of various particle sizes using SBA-15 as the template relies on the control of the combination of processing parameters such as the precursor-loading method, solvent types, and heating rate of the reduction annealing. The same amounts of precursor salts were used for all the synthetic conditions, i.e., $CoCl_2 \cdot 6H_2O$ (0.117 g, 0.4912 mmol), $Ni(NO_3)_2 \cdot 6H_2O$ (0.072 g, 0.2476 mmol), and $Ga(NO_3)_3 \cdot xH_2O$ (0.13 g, 0.325 mmol). Detailed descriptions of the synthetic procedures for Co-Ni-Ga nanoparticles of specific sizes are presented in the following paragraphs.

The 30 nm Co-Ni-Ga nanoparticles were prepared using a simple impregnation method. This included dissolving the precursor salts in deionized (DI) water (1 ml) and then adding DI water (4 ml). A slurry was obtained by adding this solution (1 ml) to SBA-15 (0.4 g) and was contained in a Petri dish. DI water (5 ml) was subsequently added to the silica slurry. The resulting solution was equalized and placed in a fume hood for drying. The dried powders were then collected. The resultant powder (200 mg) was heated under H_2 atmosphere at 10 K. min^{-1}, to 1123 K and held at this temperature for 0.1 h.

The 68 nm Co-Ni-Ga nanoparticles were prepared by dissolving the precursor salts in methanol

(50 ml) and then sonicated for 10 min. Subsequently, SBA-15 silica (1 g) was added to the precursor solution and the suspension was sonicated for another 20 min. The methanol was removed using a rotary evaporator and the resultant solid was then dried at 353 K for 8 h. The resultant powder (200 mg) was heated under H_2 atmosphere at 10 K. min^{-1}, to 1123 K and held at this temperature for 0.1 h.

The 84 nm Co-Ni-Ga nanoparticles were prepared, using 1g SBA-15 as the templates, by doubling the precursor concentration to $CoCl_2 \cdot 6H_2O$ (0.234 g, 0.98 mmol), $Ni(NO_3)_2 \cdot 6H_2O$ (0.144 g, 0.49 mmol), and $Ga(NO_3)_3 \cdot xH_2O$ (0.22 g, 0.65 mmol). The methanol was removed by a rotor evaporator and then the dried powder (200 mg) was heated under H_2 atmosphere at 10 K. min^{-1}, to 1123 K, and held at this temperature for 6 h.

1.2 X-ray diffraction

The room temperature (RT) crystal structure of Co-Ni-Ga/SBA-15 nanocomposites was investigated by using the powder X-ray diffraction (XRD) X'Pert PRO diffractometer (PANalytical B.V., Netherlands) designed in Bragg-Brentano geometry. The XRD measurements were carried out in a symmetrical θ-2θ scan mode using monochromatic Cu-$K_{\alpha 1}$ (λ = 1.540598 Å) radiation. The high temperature (HT) XRD experiment was carried out by means of powder diffractometer STOE-StadiP-MP (Stoe & Cie, Germany), designed in focusing Debye-Scherrer transmission geometry. A detailed description of the XRD experiments and data analyses is given in the electronic supplementary material (ESM) [27-36].

1.3 X-ray absorption near edge structure analysis

X-ray absorption near edge structure (XANES) spectroscopy measurements were performed at the X-ray absorption fine structure (XAFS) beamline of Elettra Sincrotrone Trieste (Trieste, Italy) and the beamline 17C1 of the National Synchrotron Radiation Research Center (NSRRC, Hsinchu, Taiwan). The Co-Ni-Ga/SBA-15 nanopowders were pressed into pellets. The Ni and Ga *K*-edge spectra of the Co-Ni-Ga nanoparticles were collected using the transmission mode. The XANES data analysis was

done using the IFEFFIT program package [37, 38]. A detailed description of the XANES experiment and data analysis is given in ESM.

1.4 Chemical analysis

The chemical composition of the the Co-Ni-Ga nanoparticles and the metal weight fractions were determined via inductively-coupled plasma optical emission spectrometer (ICP-OES, VISTA, Varian Inc.). The prepared samples were found to have the $Co_{50}Ni_{25\sim26}Ga_{23\sim30}$ compositions and the weight fractions of Co-Ni-Ga in the Co-Ni-Ga/silica nanocomposites ranged from 3.8 to 11.5 wt. %. The weight fractions of Co-Ni-Ga were obtained by a summation of the measured Co-Ni-Ga masses and divided by the overall masses of the Co-Ni-Ga/silica composites.

1.5 Nitrogen physiosorption

Nitrogen physiosorption isotherms were measured at 77 K using a Quantachrome Autosorb 1C apparatus (Quantachrome GmbH & Co. KG). Prior to the measurement, the samples were evacuated at 423 K for 5 h. Specific surface areas were calculated using the Brunauer-Emmett-Teller (BET) equation (p/p_0 = 0.05 ~ 0.2). In addition, the pore size distribution was estimated from the desorption branch of the isotherm using Density Functional Theory (DFT) and Barrett-Joyner-Halenda (BJH) methods (Figure S2 of ESM).

1.6 Transmission electron microscopy

Suspensions of SBA-15-supported Co-Ni-Ga nanoparticles were used for transition electron microscopy (TEM) sample preparation. Several drops of a suspension were loaded on carbon-coated copper grid and transferred to the microscope after being completely dried. The average size and their standard deviation of the nanoparticles were evaluated by counting more than 100 individual particles (Figure S1 of ESM). For particles of irregular shape, we determined the particle size by measuring the dimension of equivalent spheres with same areas for the irregular ones. A Tecnai 10 TEM (FEI, Eindhoven, Netherlands) equipped with a LaB_6-source at 100 kV acceleration voltage was used for the investigation of particle morphology, size distributions, and electron diffraction. Images were recorded

with a F224HD 2k slow scan CCD camera (Tietz Video and Image Processing Systems, Gauting, Germany).

1.7 Magnetic measurements

The *M-H* isothermal magnetization curves were measured at 1.8 and 300 K in fields up to 7 T in order to investigate the magnetic properties of Co-Ni-Ga nanoparticles with different particle sizes. These measurements were performed using commercial magnetometers Quantum Design MPMS-XL-7 and MPMS-3. In all these magnetic measurements, SBA-15 supported samples were used considering the diamagnetic nature of the SBA-15 silica in the measured temperature range [39]. The actual magnetization of the Co-Ni-Ga nanoparticles was calculated based on the weight fraction of the nanoparticles in the nanocomposites. All Co-Ni-Ga nanoparticle samples were fixed in quartz with molten paraffin wax in order to avoid unwanted sample movement during the measurements.

Curie temperatures of the Co-Ni-Ga nanoparticles were determined by thermomagnetic analysis (TMA), which entails measurements of the temperature-dependence of the initial susceptibility. The experiments were performed by means of a home-built alternating current (AC) susceptometer at a frequency of 500 Hz, in a wide temperature range (up to 1273 K) under an applied field of 1 mT. Curie temperatures (characterized by a drop in the signal) were determined from the inflection point of the curves. The Co-Ni-Ga/SBA-15 powders were pressed into pellets to reduce their volume.

2. Results and discussion

2.1 TEM

The sample compositions and size-dependent structural and magnetic properties of the prepared Co-Ni-Ga Heusler nanoparticles are summarized in Table 1. Co-Ni-Ga Heusler nanoparticles with sizes ranging between 30 to 84 nm were obtained using SBA-15 as templates for controlling the synthesis. Figure 1 shows TEM micrographs of the SBA-15-supported Co-Ni-Ga nanoparticles. A bimodal size distribution is observed for sample S30 with an average particle size of 30 nm (see Figure S1 of ESM).

The smaller particles are approximately 16 ± 5 nm (Figure 1(a)), which correspond to the β-phase according to the crystallite size of 12(2) nm calculated from the X-ray diffraction (XRD) data (see Table 1). The larger particles are of roughly 44 ± 10 nm (Figure 1(b)) which is close to the crystallite size, 36(1) nm, of the γ-phase (Table 1). According to Figure 1(c)-(d), the average particle sizes are 68 ± 11 and 84 ± 22 nm for the S68 and S84 samples, respectively. Thus, particles in these samples contain 2–3 crystallites (cf. TEM particle, D_{TEM}, and XRD crystallite size, D, in Table 1).

2.2 Chemical synthesis

It is very tricky to synthesize Heusler nanoparticles with desired phase and particle size. In our laboratory, we have intensively studied this silica assisted chemical approach for Heusler nanoparticles. We find that a variety of factors such as the type of Heusler compounds (Co-Fe-Ga, Co-Fe-Al, Co-Mn-Ga, Co-Ni-Ga, Ni-Fe-Ga, Mn-Fe-Ga etc.), the type of supporting materials (silica, carbon etc.), the weight fraction of nanoparticles, and hydrogen reduction annealing significantly affect the phase structure and particle size/morphology of the Heusler nanoparticles [25, 40-49]. Specific to Co-Ni-Ga nanoparticles, we have tried a library of silica supports including sol-gel silica monolith, fume silica, silica gel, colloidal silica, mesostructured cellular foam (MCF), and SBA-15. We found that γ-Co_2NiGa nanoparticles can only be prepared using colloidal silica [25]. A dual-phase structure was observed for Co-Ni-Ga nanoparticles prepared with sol-gel derived silica [48] and SBA-15 [45, 47].

Nitrogen adsorption measurements revealed that the pores of the SBA-15 are approximately 6–7 nm in diameter (see Figure S2 of ESM). Therefore, the Co-Ni-Ga nanoparticles were assumed to form only on the external surfaces of the SBA-15, similar to the formation manner of Co_2FeGa nanowires [15] and nanoparticles on certain solid substrates [50]. Although a detailed explanation for this discrepancy is not available at the moment, we believe that an appropriate choice of silica supports, a suitable weight fraction of the nanoparticles and annealing parameters are essential elements to obtain impurity-free and size-selected Co_2NiGa nanoparticles.

2.3 Crystal structure

Figure 2 shows the XRD patterns of the Co-Ni-Ga nanoparticles. The XRD patterns exhibit both, halos owing to the amorphous mesoporous SBA-15 silica, and reflections, arising from the cubic β and tetragonally distorted γ crystalline phases. The presence of both β and γ phases in all samples is consistent with the structure of the bulk Co-Ni-Ga compounds [20, 51-56]. In a Rietveld quantitative analysis we utilized the B2-structure model of the partially ordered β-phase. This choice was supported by the observation of this type of ordering of the β-phase in coexistence with the γ-phase [20]. The super-lattice reflections of the β-phase, such as *hkl* = 100 ($2\theta \approx 31.5°$) for the partially ordered B2 phase, however, were not detected by XRD. This is attributed to its weak theoretical relative intensity of 0.5 % according to the most intensive reflection (I_{max}) and also to the broadened reflections resulting from the small crystallite size and/or small scattering volumes of the β-phase, which are less than 30 vol. % in all samples. Additionally for the γ-phase in the XRD patterns, the absence of the weak (less than 1 % of I_{max}) superimposed reflections with Miller indices *hkl* = 100/001 ($2\theta \approx 24.9°$) and 110/011 ($2\theta \approx 35.4°$) can be explained by Ni-Ga site disorder in the γ-Co_2NiGa nanoparticles [25], which is enhanced by broadening of the XRD reflections due to the small crystallite sizes. The Rietveld fitting characteristics are compiled in the Table S1 of ESM. The unit cell parameters and volume fractions of these crystalline phases were derived using Rietveld quantitative analysis. The β-phase is indexed as a cubic structure (sp. gr. No. 221, $Pm\bar{3}m$, Inorganic Crystal Structure Database (ICSD) code #169729 [57]) with a mean lattice parameter of a = 2.8748(7) Å, obtained by averaging over all samples studied in current investigation. In contrast, the γ-phase has a slightly distorted tetragonal structure (sp.gr. No. 123, *P*/4*mmm,* ICSD #157788 [56]) with average lattice parameters of a = 3.585(4) Å and c = 3.572(5) Å. The composition region of the β-phase, which undergoes a martensitic transformation, is located near the β + γ region [20]. Therefore, the phase structure of bulk Co_2NiGa is preserved at the nanoscale. The Williamson-Hall plots for the reflections of both, ß- and γ-Co_2NiGa phases, prove the negligibility of microstrain broadening of the samples S30, S68 and S84 (see Figure S3 in ESM). Crystallite size analysis using the Scherrer equation indicates that the synthesized nanoparticles are composed of either one (for both crystalline phases of

sample S30), two (for the γ-phase of Sample S68), or three (for the ß-phase of S68 and both, ß- and γ-phases of S84 sample) nanocrystallites (see Table 1). The grain size calculated from quantitative Rietveld refinement displays a size-dependent pattern. For example, the crystallite size for the β-phase consistently increases with the TEM-derived particle size. This verifies the size evolution trend derived from TEM observations. Interestingly, the variation of the crystallite size for the γ-phase is not significant and the crystallite size of the γ-phase is normally larger than that of its β-phase counterpart. Furthermore, XANES analyses at the *K*-edges of Co and Ga confirmed the formation of the metallic Co-Ni-Ga phase and the absence of Co or Co oxides, which is consistent with the XRD analysis (see Figure S4 of ESM).

It is intriguing to verify whether the γ and β phases grow within the same particle or they form different particles separately. When there are two different crystalline phases with structure units characterized by similar inter-atomic distances in one crystallite, there should be an intergrowth of the phases at the boundary of the two areas with different structure. This is normally evidenced by a formation of the satellite reflections or at-least shoulders of the main high-intensive XRD reflections [58-61]. No such satellite reflection was observed in the XRD patterns and it was proved by a good quality of fits of the XRD patterns using Rietveld method. Thus, most likely, the γ and β phases form different particles separately, and one particle may have multiple crystal domains but a single phase. It is noted that the same situation is also applied for the sample S30 where particles of various sizes correspond to various phases, respectively,

Size dependent crystal structure of nanostructured materials is an important issue in Nanoscience and Nanotechnology. There have been many studies for conventionally metallic, ceramic, shape memory and other nanoparticles. Size-dependent structure of Co-Ni-Ga nanoparticles, however, has not been studied prior to this work. In this work, we investigate the size-dependent crystal structure concerning γ/β ratio. According to results of quantitative Rietveld refinement (see Table 1), the γ/β ratios for samples S30, S68, and S84 were calculated as 4.81, 2.47, and 2.76, respectively. Hence it is observed

that the γ/β ratio decrease with increasing particle size in the range of 30-84 nm. For relatively larger nanoparticles (e.g. for S68 and S84), however, the difference in γ/β ratio is less affected by the particle size. This argument is also supported by the results of β-phase dominated Co-Ni-Ga nanoparticles published in our recent work [48]. When the γ/β ratio is less than 1 (i.e. more β phase than γ phases), the γ/β ratio also decreases with increasing particle size, i.e. 0.47 and 0.09 corresponding to 90 nm and 110 nm, respectively. Therefore, it is concluded that the γ/β ratio decreases with increasing particle size. Size reduction induced variations in lattice symmetry have been intensively studied for metal oxide nanoparticles [62]. It was observed that the crystal lattice of selected oxides (e.g. $BaTiO_3$) tends to transform into a structure for higher symmetry with decreasing crystal size below a critical particle size [63]. There exist, however, limited investigation on similar behavior of metallic and alloyed nanoparticles. Here we first observed the size-dependent phase structure of Co-Ni-Ga nanoparticles but the mechanism of the observed behavior is unclear for the moment. It is generally assumed that only small metallic nanoparticles (e.g. ~10-20 nm) exhibit a significant size-dependent crystal structure [64-69]. It is not expected that the variation in γ/β ratio is simply due to the contribution of the size effect because of the relatively broad size distribution and the co-existence of particles of various morphologies (as described above). In addition, the tetragonality ratio *c/a* of the γ-phase of Co-Ni-Ga nanoparticles is close to 1 (see Table 1), which adds technical difficulty in probing the potential lattice transformation as a function of particle size. To elucidate how and why the particle size affects the γ/β ratio, a successful preparation of nanoparticles with desired phases and particle size is essential, which is an objective of further investigations.

2.4 Magnetic properties

Figure 3 shows the field-dependent magnetization curves of the Co-Ni-Ga nanoparticles measured at 2 K. The nanoparticles all demonstrate ferromagnetic properties. The saturation magnetization (M_s), given as the magnetic moment (μ_B) per formula unit, increases with increasing

particle size: 1.81, 2.29, and 2.90 μ_B for nanoparticles with sizes of 30, 68, and 84 nm, respectively. A reverse trend is observed in the coercivity ($\mu_o H_c$) and remanence (M_r). Both $\mu_o H_c$ and M_r decrease with increasing particle size, at 115.85, 49.60, and 39.80 mT for the former and 0.80, 0.79, and 0.57 μ_B for the latter for particles of 30, 68, and 84 nm in size, respectively. The coercivity of sample S30 is comparable to that (≈ 100 mT) of $Co_{50}Ni_{20}Ga_{30}$ ribbons [24], which is attributed to the formation of fine β and γ phases. The size-dependent M_s, $\mu_o H_c$, and M_r of the Co-Ni-Ga nanoparticles are consistent with those reported for magnetic nanoparticles [70-72], thereby confirming the formation of size-controlled Co-Ni-Ga Heusler nanoparticles.

The Curie temperatures (T_c) of the Co-Ni-Ga nanoparticles were estimated by temperature-dependent AC susceptibility measurements under an applied field of 1.5 mT. As shown in Figure 4 presenting the results of TMA measurements, significant drops are observed in the magnetic susceptibility curves. These signals reflect a ferromagnetic-paramagnetic transition of the Co-Ni-Ga nanoparticles. The Curie temperatures, as determined by the inflection points, are 1073 K, 1143 K and 1174 K for samples S30, S68 and S84, respectively. Hence, the T_c of the Co-Ni-Ga nanoparticles decreases with decreasing particle sizes, exhibiting a pronounced size effect. It is also noted that the T_c of sample S30 shows a hysteretic behavior: the paramagnetic phase appears at 1124 K on heating, while an undercooling of approximately 50 K is required to restore ferromagnetism in this sample. This behavior might be also related to a partial degradation of the nanoparticles due to the prolonged exposure to a high temperature during the measurement. Furthermore, the difference in susceptibility between the heating and cooling branches shown in Figure 4 is probably due to different rearrangements of the magnetic domains while crossing the Curie transition in an applied field.

The size-dependency of the T_c in magnetic nanoparticles has been investigated mostly for single-phase metallic or oxide materials [70-72]. Here we report the size dependence of the T_c in dual-phase Co-Ni-Ga nanoparticles. The observed scaling laws for single-phase nanoparticles indicate a proportional relationship between T_c and particle size. For example, Ni nanoparticles of 23, 80, and 114 nm have a T_c of

610 K, 625 K, and 627 K, respectively. These are slightly lower than the T_c (631 K) for bulk Ni [72]. Here, the observed T_c of the Co-Ni-Ga nanoparticles are much higher than those reported for single-crystal Co-Ni-Ga thin films (≈ 670 K) [73] or polycrystalline Co-Ni-Ga melt-spun ribbon (up to 950 K) [24]. To our knowledge, the measured T_c (1174 K) of the 84 nm Co-Ni-Ga nanoparticles (sample S84) is the highest among all known Heusler compounds. The observed very high T_c of the Co-Ni-Ga nanoparticles reflects a complicated interaction of a material's synthetic method, composition and the formation of nanocomposite. Specifically, several aspects may be important to account for the observed extraordinary magnetic properties.

First, the sample preparation method might affect the magnetic properties of dual-phase Co-Ni-Ga nanoparticles. For example, the melt-spun $Co_{50}Ni_{20}Ga_{30}$ dual-phase ribbons showed a higher T_c (~950 K) than that (~390 K) of $Co_{50}Ni_{20}Ga_{30}$ bulk samples prepared by conventional arc-melting methods. In this work, the T_c of the Co-Ni-Ga nanoparticles are significantly higher than those of Co-Ni-Ga bulk samples with similar phase structures. The reason for the preparation method induced differences in magnetic characteristics is unknown. Probably the difference is arising from different microstructures for the studied samples. The magnetic properties of Co-Ni-Ga nanoparticles are affected by the particle size, but are also strongly influenced by other factors such as particle morphology and inter-particle magnetic interactions. For example, as illustrated in Figure S9, we find by TEM that some non-spherical nanoparticles as well as nanorods/nanowires co-exist with the spherical particles. The presence of "irregular" particles was attributed to the unique SBA-15 silica assisted chemical approach developed in this work. The above factors make the studies of a collection of Co-Ni-Ga nanoparticles very complicated and several parameters have to be taken into account. To distinguish the effect of particle size from those of morphology, Co-Ni-Ga nanoparticles with a very narrow particle size distribution or clearly defined shape are required. We realize that the above requirements are very challenging for materials scientist and deserve future investigations. In addition, the Co-Ni-Ga materials have a non-stoichiometric composition, especially with respect to the Ga content. As observed in this work, the

T_c of the Co-Ni-Ga nanoparticles steadily increases with decreasing Ga content. Unfortunately, there exist limited reports on the T_c of bulk samples with compositions similar to the Co-Ni-Ga nanoparticles studied here. To clarify the effect of Ga, further experimental studies on bulk Co-Ni-Ga samples with a variation in Ga would be necessary.

Second, structural factors such as γ/β ratio might also affect the magnetic properties of Co-Ni-Ga nanoparticles. The γ/β ratios are calculated as 4.81, 2.47 and 2.76 for samples with particle size of 30, 68 and 84 nm, respectively. Hence it is observed that T_c increases with decreasing γ/β ratio in the studied size range. For relatively larger nanoparticles (e.g. for S68 and S84), however, the difference in γ/β ratio is small (approximately 2 vol. %) and T_c is more affected by the particle size (68 nm/1143 K vs 84 nm/1173 K). Thus, it seems that the effects of γ/β ratio and particle size on T_c are correlated and cannot be separated clearly from each other. This argument is also supported by the results published in our recent work [48]. The samples A54-05 and A30-05 show γ/β ratios of 0.47 and 0.09, respectively. In the same time, the samples are characterized by increasing particle size and decreasing T_c: 90 nm/1153 K vs 110 nm/998 K. Therefore, for relatively large particle and when the γ/β ratio is less than 1 (i.e. more β phase than γ phases), T_c increases with increasing γ/β ratio and decreasing particle size. To unambiguously clarify how the γ/β ratio affects T_c beside the size effect, more influencing factors such as particle size range, preparation method and phase composition also need to be taken into consideration. What's more, a successful preparation of nanoparticles with desired phases and particle size is essential, which poses a tough challenge to materials scientists.

Furthermore, the observed high T_c might be also related to the silica/nanoparticle composites. Our recent studies have revealed a high T_c (~ 1139 K) for γ-phase Co_2NiGa nanoparticles [25] and a T_c of 998 K for the "almost" single-β phase $Co_{50}Ni_{18}Ga_{32}$ nanoparticles (with a phase structure of 91.4 vol.% β + 8.6 vol. % γ) [48]. Thus, a simple mixture of γ- and β-phase nanoparticles is not probable to further increase the T_c of the dual-phase nanoparticles to ~1174 K. On the other hand, it has been intensively investigated and proved that the T_c of ferromagnets may be tuned by the construction of composite

materials [74]. If the magnetic moments of a ferromagnetic phase are aligned parallel to each other, the T_c increases, as more thermal energy is required to destroy long-range magnetic ordering. In the present investigation, the Co-Ni-Ga nanoparticles were assumed to form on the external surfaces of highly ordered SBA-15 silica. It is feasible that the immobilized nanoparticles pack or assemble in an orderly fashion within certain confined spaces of the SBA-15 silica. This may promote the alignment of magnetic moments, possibly, by exchange interactions [75]. As a result, the degree of the magnetic ordering is drastically enhanced.

More importantly, the observed extraordinarily high T_c of the Co-Ni-Ga nanoparticles might be related to the presence of Co-like phases during the heating process of TMA measurements, which also show very high T_c. Therefore, we additionally performed HT XRD measurements on the sample S84 to detect probable phase transition or the presence of Co-like phases in the dual-phase Co-Ni-Ga nanoparticles. As shown in Figure 5 for the sample S84, an irreversible phase transition of the ß-phase was observed starting at temperature of about 837 K, resulting in the formation of an amorphous phase. In comparison, the structural symmetry of the γ-phase was stable upon heating to 1028 K. In the cooling process down to 298 K, a preservation of the structure symmetry with reduced unit cell parameters was observed for the γ-phase. It should be noted, however, that the γ-phase reflections can be indexed alternatively as the reflections of the cubic $Co_{1-x}Ni_x$ phase (space group No. 225, $Fm\bar{3}m$) with an excess of Co (correspondingly, the reflections with *hkl* = 111, 200 and 220 at 2θ = 44.26°, 51.57° and 75.82°). In this case, the calculated unit cell parameters (a = 3.5443(15) Å) become close to that of pure Co (a = 3.544 Å [76], ICSD 76632). Therefore, preliminary HT XRD results reveal both phase transition (ß-phase) and the possible presence of the Co-like phases, which might contribute to the observed high T_c of the dual-phase Co-Ni-Ga nanoparticles. Due to the low statistically resolved data, however, Rietveld refinement analysis of the structure including atomic site occupancies cannot be performed. The temperature-dependent variations in unit cell parameter a, unit cell volume V_{cell} and crystallite size D of

the sample S84 are described in Figures S6-S7 of ESM. Further HT investigations using high-resolution synchrotron sources are required to verify the formation of the Co phase after high temperature treatment.

3. Conclusion

In summary, size-selected Co-Ni-Ga nanoparticles were chemically prepared using SBA-15 as a template and proven using complementary techniques of XRD, XANES and TEM. The size-dependent phase structure and magnetic properties of the shape memory Heusler Co-Ni-Ga nanoparticles were investigated. The Co-Ni-Ga nanoparticles exhibited enhanced saturation magnetization, decreased coercivity, and enhanced T_c with increasing particle sizes in the range of 30–84 nm. High temperature XRD measurements reveal the phase transition and possible presence of the Co-like phase, which probably account for the observed high T_c in the dual-phase Co-Ni-Ga nanoparticle. Further theoretical and experimental investigations are desired for this new class, size-selected shape memory Heusler nanoparticles.

Acknowledgements

We acknowledge financial supports by the German Research Foundation (DFG) under the Project of TP 2.3-A in research unit FOR 1464 ‘ASPIMATT’ and the ERC Advanced Grant (291472 Idea Heusler).The authors are also grateful to: Prof. A. Hütten (Department of Physics, Bielefeld University) for stimulating discussions; Dr. R. Ramlau and Ms. U. Köhler (MPI-CPfS) for TEM support; Dr. G. Auffermann (MPI-CPfS) for the chemical analysis; Dr. H. Borrmann (MPI-CPfS) for support of the HTXRD measurements; Prof. S. Kaskel (Department of Inorganic Chemistry, Technical University of Dresden) for the nitrogen adsorption measurements; Mr. R. Koban for kind help with sample preparation and magnetic measurements; Dr. L. Olivi (Elettra Sincrotrone Trieste) for stimulating discussion and kind help with the XANES experiments. The XANES measurements were performed at the Elettra Sincrotrone Trieste (Trieste, Italy) under the approval of proposal No. 20140471 and at the

National Synchrotron Radiation Research Center (NSRRC, Hsinchu, Taiwan) under the approval of proposal No. 2013-2-027-4.

Electronic Supplementary Materials

Supplementary material (TEM-derived particle size distribution, N_2 physiosorption data, detailed descriptions on XANES, RT/HT XRD experiment and discussions, additional TEM micrograph) is available in the online version of this articles.

References

[1] Saxena, A.; Aeppli, G. Phase Transitions at the Nanoscale in Functional Materials. *MRS. Bull.* **2009**, *34*, 804-813.

[2] Waitz, T.; Tsuchiya, K.; Antretter, T.; Fischer, F. D. Phase Transformations of Nanocrystalline Martensitic Materials. *MRS. Bull.* **2009**, *34*, 814-821.

[3] San Juan, J. M.; Nó, M. L.; Schuh, C. A. Nanoscale Superelastic Alloys with Ultra-High Damping Capacity. *Nat. Nanotechnol.* **2009**, *4*, 415-419.

[4] Zhang, J.; Ke, X.; Gou, G.; Seidel, J.; Xiang, B.; Yu, P.; Liang, W.-I.; Minor, A. M.; Chu, Y.-H.; Tendeloo, G. V.; Ren, X.; Ramesh, R. A Nanoscale Shape Memory Oxide. *Nat. Commun.* **2013**, *4*, 2768.

[5] Liu, Y.; Karaman, I.; Wang, H.; Zhang, X. Two Types of Martensitic Phase Transformations in Magnetic Shape Memory Alloys by In-Situ Nanoindentation Studies. *Adv. Mater.* **2014**, *26*, 3893-3898.

[6] Waitz, T; Antretter, T.; Fischer, F. D.; Simha, N. K.; Karnthaler, H. P. Size Effects on the Martensitic Phase Transformation of NiTi Nanograins. *J. Mech. Phys. Solids* **2007**, *55*, 419-444.

[7] Glezer, A. M.; Blinova, E. N.; Pozdnyakov, V. A.; Shelyakov, A. V. Martensite Transformation in Nanoparticles and Nanomaterials. *J. Nanopart. Res.* **2003**, *5*, 551-560.

[8] Waitz, T.; Kazykhanov, V.; Karnthaler, H. P. Martensitic Phase Transformations in Nanocrystalline NiTi Studied by TEM. *Acta Mater.***2004**, *52*, 137-147.

[9] Waitz, T.; Spišák, D.; Hafner, J.; Karnthaler, H. P. Size-Dependent Martensitic Transformation Path Causing Atomic-Scale Twinning of Nanocrystalline NiTi Shape Memory Alloys. *Europhys. Lett.***2005**, *71*, 98-103.

[10] Waitz, T.; Pranger, W.; Antretter, T.; Fischer, F. D.; Karnthaler, H. P. Competing Accommodation Mechanisms of the Martensite in Nanocrystalline NiTi Shape Memory Alloys. *Mater. Sci. Eng. A* **2008**, *481-482*, 479-483.

[11] Zhao, X.; Liang, Y.; Hu, Z.; Liu, B. Thermodynamic Interpretation of the Martensitic Transformation in Ultrafine γ-Fe(N) Particles. *Jpn. J. Appl. Phys.* **1996**, *35*, 4468-4473.

[12] *Wang*, Y. D.; Ran, Y.; Nye, H. Z.; Liu, D. M.; Coho, L.; Zoo, H.; Li, H.; Law, P. K.; Yan, J. Q.; McQueen, R. J.; Richardson, J. W.; Hu, A. Structural Transition of Ferromagnetic Ni_2MnGa Nanoparticles. *J. Appl. Phys.* **2007**, *101*, 063530.

[13] Liu, D. M.; Nie, Z. H.; Wang, Y. D.; Liu, Y. D.; Wang, G.; Ren, Y.; Zuo, L. New Sequences of Phase Transition in Ni-Mn-Ga Ferromagnetic Shape Memory Nanoparticles. *Metall. Mater. Trans. A* **2008**, *39A*, 466-469.

[14] Seki, K.; Kura, H.; Sato, T.; Taniyama, T. Size Dependence of Martensite Transformation Temperature in Ferromagnetic Shape Memory Alloy FePd. *J. Appl. Phys.* **2008**, *103*, 063910.

[15] Simon, P.; Wolf, D.; Wang, C.; Levin, A. A.; Sturm, S.; Lichte, H.; Qian, J.; Fecher, G. H.; Felser, C. Synthesis and Three-Dimensional Magnetic Field Mapping of Co_2FeGa Heusler Nanowires at 5 nm Resolution. *Nano Lett.***2016**, *16*, 114-120.

[16] Imperor-Clerc, M.; Bazin, D.; Appay, M.-D.; Beaunier, P.; Davidson, A. Crystallization of β-MnO_2 Nanowires in the Pores of SBA-15 Silica: In-situ Investigation Using Synchrotron Radiation. *Chem. Mater.* **2004**, *16*, 1813-1821.

[17] Zhang, F.; Lam, L.-Y.; Hu, X.; Yang, Z.; Sheng, P. Reaction Paths between $LiNH_2$ and LiH with Effects of Nitrides. *J. Phys. Chem. C* **2007**, *111*, 12531-12536.

[18] Kockrick, E.; Krawiec, P.; Schnelle, W.; Geiger, D.; Schappacher, F. M.; , R.; Kaskel, S. Space-Confined Formation of FePt Nanoparticles in Ordered Mesoporous Silica SBA-15. *Adv. Mater.* **2007**, *19*, 3021-3026.

[19] He, M.; Wong, C. H.; Tse, P. L.; Zheng, Y.; Zhang, H.; Lam, F. L. Y.; Sheng, P.; Hu, X.; Lortz, R. "Giant" Enhancement of the Upper Critical Field and Fluctuations above the Bulk T_c in Superconducting Ultrathin Lead Nanowire Arrays. *ACS Nano* **2013**, *7*, 4187-4193.

[20] Dogan, E.; Karaman, I.; Chumlyakov, Y. I.; Luo, Z. P. Microstructure and Martensitic Transformation Characteristics of CoNiGa High Temperature Shape Memory Alloys. *Acta Mater.***2011**, *59*, 1168-1183.

[21] Dadda, J.; Maier, H. J.; Niklasch, D.; Karaman, I.; Karaca, H. E.; Chumlyakov, Y. I. Pseudoelasticity and Cyclic Stability in $Co_{49}Ni_{21}Ga_{30}$ Shape-Memory Alloy Single Crystals at Ambient Temperature. *Metall. Mater. Trans. A* **2008**, *39*, 2026-2039.

[22] Craciunescu, C.; Kishi, Y.; Lograsso, T. A.; Wuttig, M. Martensitic Transformation in Co_2NiGa Ferromagnetic Shape Memory Alloys. *Scripta Mater.***2002**, *47*, 285-288.

[23] Fu, H.; Yu, H.J.; Teng, B.H.; Zhang, X.Y.; Zu, X. T. Magnetic Properties and Magnetic Entropy Change of $Co_{50}Ni_{22}Ga_{28}$ Alloy. *J. Alloys Compd.* **2009**, *474*, 595-597.

[24] Saito, T.; Koshimaru, Y.; Kuji, T. Structures and Magnetic Properties of Co–Ni–Ga Melt-spun Ribbons. *J. Appl. Phys.* **2008**, *103*, 07B322.

[25] Wang, C.; Levin, A. A.; Fabbrici, S.; Qian, J.; Schnelle, W.; Albertini, F.; Fecher, G. H.; Felser, C. Chemical Synthesis and Characterization of γ‑Co_2NiGa Nanoparticles with a Very High Curie Temperature. *Chem. Mater.***2015**, *27*, 6994-7002.

[26] Zhao, D. Y.; Huo, Q. S.; Feng, J. L.; Chmelka, B. F.; Stucky, G. D. Nonionic Triblock and Star Diblock Copolymer and Oligomeric Surfactant Synthesis of Highly Ordered, Hydrothermally Stable, Mesoporous Silica Structures. *J. Am. Chem. Soc.* **1998**, *120*, 6024-6036.

[27] Levin, A. A.; Levichkova, M.; Hildebrandt, D.; Klisch, M.; Weiss, A.; Wynands, D.; Elschner, C.; Pfeiffer, M.; Leo, K.; Riede, M. Effect of Film Thickness, Type of Buffer Layer, and Substrate Temperature on the Morphology of Dicyanovinyl-Substituted Sexithiophene Films. *Thin Solid Films* **2012**, *520*, 2479-2487.

[28] Program ANALYZE, Rayflex Version 2.285, Rich. Seifert & Co., **2000**.

[29] Langford J. I. Accuracy of crystallite size and strain determined from the integral breadth of powder diffraction lines in *Accuracy in Powder Diffraction*. Block, S.; Hubbard, C. R. eds. , Nat. Bur. Stand. Spec. Pub. No. 567, National Bureau of Standards: Washington, **1980**: pp 255-269.

[30] Rehani, B. R.; Joshi, P. B.; Lad, K. N.; Pratap, A. Crystallite Size Estimation of Elemental and Composite Silver Nano-Powders using XRD Principles. *Indian J. Pure Appl. Phys.* **2006**, *44*, 157-161.

[31] Terlan, B.; Levin, A. A.; Börrnert, F.; Simon, F.; Oschatz, M.; Schmidt, M.; Cardoso-Gil, R.; Lorenz, T.; Baburin, I. A. ; Joswig, J. O. ; Eychmüller, A. Effect of Surface Properties on the Microstructure, Thermal, and Colloidal Stability of VB_2 Nanoparticles. *Chem. Mater.* **2015**, *27*, 5106-5115.

[32] Akselrud, L.; Grin, Y. *WinCSD*: Software Package for Crystallographic Calculations (Version 4). *J. Appl. Crystallogr.* **2014,** *47***,** 803-805.

[33] Bérar, J.-F.; Lelann, P. E.s.d.'s and Estimated Probable Error Obtained in Rietveld Refinements with Local Correlations. *J. Appl. Crystallogr.* **1991**, *24*, 1-5.

[34] Levin, A. A.; Filatov, S. K.; Paufler, P.; Bubnova, R. S.; Krzhizhanovskaya, M.; Meyer, D. C. Temperature-dependent Evolution of $RbBSi_2O_6$ Glass into Crystalline Rb-boroleucite According to X-ray Diffraction Data. *Z. Kristallogr.* **2013**, *228*, 259-263.

[35] Young, R. A. *Introduction to the Rietveld Method*, IUCr Book Series, Oxford University Press: 1993; pp 21-24.

[36] C. Maunders, J. Etheridge, N. Wright, H. J. Whitfield, Structure and Microstructure of Hexagonal $Ba_3Ti_2RuO_9$ by Electron Diffraction and Microscopy. *Acta Cryst.* **2005**, *B61*, 154.

[37] Newville, M.; Ravel, B.; Haskel, B. D.; Rehr, J. J.; Stern, E. A.; Yacoby, Y. Analysis of Multiple-Scattering XAFS Data using Theoretical Standards. *Physica B* **1995**, *208*,154-156.

[38] Newville, M. IFEFFIT: Interactive XAFS Analysis and FEFF Fitting. *J. Synchrotron Radiat.* **2001**, *8*, 322-324.

[39] Zeleňák, V.; Zeleňáková, A.; Kováč, J. Insight into Surface Heterogenity of SBA-15 Silica: Oxygen Related Defects and Magnetic Properties. *Colloids Surf. A: Physicochem. Eng. Aspects* **2010**, *357*, 97-104.

[40] Basit, L.; Wang, C.; Jenkins, C. A.; Balke, B.; Ksenofontov, V.; Fecher, G. H.; Felser, C.; Mgnaioli, E.; Kolb, U.; Nepijko, S. A.; Schönhense, G.; Klimenkov, M. Heusler compounds as ternary intermetallic nanoparticles: Co_2FeGa. J. *Phys. D Appl. Phys.***2009**, *42*, 084018.

[41] Wang, C.; Guo, Y.; Casper, F.; Balke, B.; Fecher, G. H.; Fesler, C.; Hwu, Y. Size correlated long and short range order of ternary Co_2FeGa Heusler nanoparticles. *Appl. Phys. Lett.* **2010**, *97*, 103106.

[42] Wang, C.; Basit, L.; Khalayka, Y.; Guo, Y.; Casper, F.; Gasi, T.; Ksenofontov, V.; Balke, B.; Fecher, G. H.; Sönnichsen, C.; Hwu, Y.; Lee, J. J.; Felser, C. Probing the size effect of Co_2FeGa-SiO_2@C nanocomposite particles prepared by a chemical approach. *Chem. Mater.* **2010**, *22*, 6575-6582

[43] Wang, C.; Casper, F.; Guo, Y.; Gasi, T.; Ksenofontov, V.; Balke, B.; Fecher, G. H.; Felser, C.; Hwu, Y. K.; Lee, J. J. Resolving the phase structure of nonstoichiometric Co_2FeGa Heusler nanoparticles. *J. Appl. Phys.* **2012**, *112*, 124314.

[44] Wang, C.; Casper, F.; Gasi, T.; Ksenofontov, V.; Balke, B.; Fecher, G. H.; Felser, C.; Hwu, Y. K.; Lee, J. J. Structural and magnetic properties of Fe_2CoGa Heusler nanoparticles. *J. Phys. D Appl. Phys.* **2012**, *45*, 295001.

[45] Wang, C.; Meyer, J.; Teichert, N.; Auge, A.; Rausch, E.; Balke, B.; Hütten A.; Fecher, G. H.; Felser, C. Heusler nanoparticles for spintronics and ferromagnetic shape memory alloys. *J. Vac. Sci. Technol. B* **2014**, *32*, 020802.

[46] Lubt, A.; Wolf, D.; Simon, P.; Wang, C.; Sturm, S.; Felser, C. Nanoscale three-dimensional reconstruction of electric and magnetic stray fields around nanowires. *Appl. Phys. Lett.* **2014**, *105*, 173110.

[47] Fichtner, T.; Wang, C.; Levin, A. A.; Kreiner, G.; Meijia, C. S.; Fabbrici, S.; Albertini, F.; Felser, C. Metals, Effects of annealing on the martensitic transformation of Ni-based ferromagnetic shape memory Heusler alloys and nanoparticles *Metals* **2015**, *3*, 100102.

[48] Wang, C.; Levin, A. A.; Fabbrici, S.; Nasi, L.; Karel, J.; Qiang, J. F.; Barbosa, C. E. V.; Ouardi, S.; Albertini, F.; Schnelle, W.; Borrmann, H.; Fecher, G. H.; Felser, C. Tunable Structural and Magnetic Properties of Chemically Synthesized Dual-phase Co_2NiGa Nanoparticles. *J. Mater. Chem. C.* **2016**, *4*, 7241-7252.

[49] Simon, P.; Wolf, D.; Wang, C.; Levin, A. A.; Sturm, S.; Lichte, H.; Fecher, G. H.; Felser, C. Synthesis and three-dimensional magnetic field mapping of Co_2FeGa Heusler nanowires at 5 nm resolution. *Nano Lett.* **2016**, *16*, 114-120.

[50] Xia, Y.; Yang, P.; Sun, Y.; Wu, Y.; Mayers, B.; Gates, B.; Yin, Y.; Kim, F.; Yan, H. One-Dimensional Nanostructures: Synthesis, Characterization, and Applications. *Adv. Mater.* **2003**, *15*, 353-389.

[51] Sato, M.; Okazaki, T.; Furuya, Y.; Wuttig, M. Magnetostrictive and Shape Memory Properties of Heusler Type Co_2NiGa Alloys. *Mater. Trans.* **2003**, *44*, 372-376.

[52] Sato, M.; Okazaki, T.; Furuya, Y.; Kishi, Y.; Wuttig, M. Phase Transformation and Magnetic Property of Heusler Type Co_2NiGa Alloys. *Mater. Trans.* **2004**, *45*, 204-207.

[53] Brown, P. J.; Ishida, K.; Kainuma, R.; Kanomata, T.; Neumann, K.-U.; Oikawa, K.; Ouladdiaf, B.; Ziebeck, K. R. A. Crystal Structures and Phase Transitions in Ferromagnetic Shape Memory Alloys Based on Co-Ni-Al and Co-Ni-Ga. *J. Phys. Condens. Mat.* **2005**, *17*, 1301-1310.

[54] Dai, X. F.; Wang, H. Y.; Liu, G. D.; Wang, Y. G.; Duan, X. F.; Chen, J. L.; Wu, G. H. Effect of Heat Treatment on the Properties of $Co_{50}Ni_{20}Ga_{30}$ Ferromagnetic Shape Memory Alloy Ribbons. *J. Phys. D Appl. Phys.* **2006**, *39*, 2886-2889.

[55] Oikawa, K.; Ota, T.; Imano, Y.; Omori, T.; Kainuma, R.; Ishida, K. Phase Equilibria and Phase Transformation of Co-Ni-Ga Ferromagnetic Shape Memory Alloy System. *J. Phase Equilib. Diff.* **2006**, *27*, 75-82.

[56] Dai, X. F.; Liu, G. D.; Li, Y. X.; Qu, J. P.; Li, J.; Chen, J. L.; Wu, G. H. Structure and Magnetic Properties of Highly Ordered Co_2NiGa alloys. *J. Appl. Phys.* **2007**, *101*, 09N503.

[57] Arroyave, R.; Junkaew, A.; Chivukula, A.; Bajaj, S.; Yao, C.-Y.; Garay, A. Investigation of the Structural Stability of Co_2NiGa Shape Memory Alloys via Ab Initio Methods. *Acta Mater.***2010**, *58*, 5220-5231.

[58] Meyer, D. C., Levin, A. A., Leisegang, T.; Gutmann, E.; Paufler, P.; Reibold, M. Reversible Tuning of a Series of Intergrowth Phases of the Ruddlesden-Popper Type $SrO(SrTiO_3)_n$ In An (001) $SrTiO_3$ Single-Crystalline Plate By An External Electric Field and Its Potential Use for Adaptive X-ray Optics. *Appl. Phys. A* **2006**, *84*. 31-35.

[59] Meyer, D. C.; Paufler, P. Coherency and Lattice Spacings of Textured Permalloy/Copper Multilayers as Revealed by X-ray Diffraction. *J. Alloys Compd.* **2000**, *298*, 42-46.

[60] Segmüller, C.; Blakeslee, A. X-ray Diffraction from One-Dimensional Superlattices in $GaAs_{1-x}P_x$ Crystals. *J. Appl. Cryst.* **1973**, *6*, 19-25.

[61] Michaelsen, C. On the Structure and Homogeneity of Solid Solutions: The Limits of Conventional X-ray Diffraction. *Philos. Mag. A* **1995**, *72*, 813-828.

[62] Ayyub, P.; Palkar, V. R.; Chattopadhyay, S.; Multani, M. Effect of Crystal Size Reduction on Lattice Symmetry and Cooperative Properties. *Phys. Rev. B.* **1995**, *51*, 6135-6138.

[63] Uchino, K.; Sadanaga, E.; Hirose, T. Dependence of the Crystal Structure on Particle Size in Barium Titanate. *J. Am. Ceram. Soc.***1989**, *72* 1555-1558.

[64] Teranishi, T.; Miyake, M. Size Control of Palladium Nanoparticles and Their Crystal Structures. *Chem. Mater.* **1998**, *10*, 594-600.

[65] Takahashi, Y.; Koyama, T.; Ohnuma, M.; Ohkubo, T.; Hono, K. Size Dependence of Ordering in FePt Nanoparticles. *J. Appl. Phys.* 2004, 95, 2690-2696.

[66] Qi, W.; Wang, M. Size and Shape Dependent Lattice Parameters of Metallic Nanoparticles. *J. Nanopart. Res.* **2005**, *7*, 51-57.

[67] Baletto, F.; Ferrando, R. Structural Properties of Nanoclusters: Energetic, Thermodynamic, and Kinetic Effects. *Rev. Mod. Phys.* 2005, 77, 371-423.

[68] Rong, C.; Li, D.; Nandwana, V.; Poudyal, N.; Ding, Y.; Wang, Z.; Zeng, H.; Liu, J. Size-Dependent Chemical and Magnetic Ordering in $L1_0$-FePt Nanoparticles. *Adv. Mater.* **2006**, *18*, 2984-2988.

[69] Wu, S.; Jiang, Y.; Hu, L.; Sun, J.; Wan, P.; Sun, L. Size-Dependent Crystalline Fluctuation and Growth Mechanism of Bismuth Nanoparticles under Electron Beam Irradiation. *Nanoscale* **2016**, *8*, 12282-12288.

[70] Jun, Y.-W.; Seo, J.-W.; Cheon, J. Nanoscaling Laws of Magnetic Nanoparticles and Their Applicabilities in Biomedical Sciences. *Acc. Chem. Res.* **2008**, *41(2)*, 179-189.

[71] Willard, M. A.; Kurihara, L. K.; Carpenter, E. E.; Calvin, S.; Harris, V. G. Chemically Prepared Magnetic Nanoparticles. *Int. Mater. Rev.* **2004**, *49(3-4)*, 125-170.

[72] He, X. M.; Zhong, W.; Au, C.-T.; Du, Y. W. Size Dependence of the Magnetic Properties of Ni Nanoparticles Prepared by Thermal Decomposition Method. *Nanoscale Res. Lett.* **2013**, *8*, 446.

[73] Shih, T. C.; Xie, J. Q.; Dong, J. W.; Dong, X. Y.; Srivastava, S.; Adelmann, C.; Makernan, S.; James, R. D.; Palmstrøm, C. J. Epitaxial Growth and Characterization of Single Crystal Ferromagnetic Shape Memory Co_2NiGa Films. *Ferroelectrics.* **2006**, *342(1)*, 35-42.

[74] Hernando, A.; Navarro, I.; Prados, C.; Garcia, D.; Vazquez, M.; Alsonso, J. Curie-Temperature Enhancement of Ferromagnetic Phases in Nanoscale Heterogeneous Systems. *Phys. Rev. B* **1996**, *53*, 8223.

[75] Lopez-Dominguez, V.; Hernàndez, J. M.; Tejada, J.; Ziolo, R. F. Colossal Reduction in Curie Temperature Due to Finite-Size Effects in $CoFe_2O_4$ Nanoparticles. *Chem. Mater.* **2013**, *25*, 6-11.

[76] A. Taylor, R.W. Floyd. Precision Measurements of Lattice Parameters of Non-Cubic Crystals. *Acta Cryst.* **1950**, *3*, 285-289.

Table 1. Sample nominal composition, particle size D_{TEM} from TEM, crystal structure (unit cell parameters *a* and *c*),[a] crystallite size *D* from XRD,[b] volume phase fraction *Vol*,[c] and magnetic properties (saturation magnetization M_s, coercivity $\mu_o H_c$, remanence M_r, and Curie temperature T_c) of the Co-Ni-Ga nanoparticles. The estimated standard deviations (e.s.d.s) of the obtained values are shown in brackets.

ID	Composition /D_{TEM} (nm)	Crystal structure and microstructure							Magnetic properties			
		β			*γ*							
		a (Å)	*Vol.* (%)	*D* (nm)	*a* (Å)	*c* (Å)	*Vol.* (%)	*D* (nm)	M_s[d] (μ_B)	$\mu_o H_c$[d] (mT)	M_r[d] (μ_B)	T_c (K)
S30	$Co_{50}Ni_{26}Ga_{30}$ /16±5,44±10[e]	2.8755(6)	17.2(5.4)	12(2.0)	3.5891(5)	3.565(2)	82.8(5.4)	36(1.0)	1.81	115.85	0.80	~1123
S68	$Co_{50}Ni_{26}Ga_{28}$ /68±11	2.8747(2)	28.8(1.0)	20(4.0)	3.5831(7)	3.576(2)	71.2(1.0)	31(7.0)	2.29	49.60	0.79	1143
S84	$Co_{50}Ni_{25}Ga_{23}$ /84±22	2.8739(2)	26.6(1.9)	36(6.0)	3.5815(4)	3.576(9)	73.4(1.9)	31(3.0)	2.90	39.80	0.57	1174

[a] According to results of quantitative Rietveld refinement; see XRD section of ESM.
[b] According to results of XRD microstructure analysis; see XRD section of ESM.
[c] The volume fractions *Vol* are recalculated from the weight fractions (*Wt)* according to equation $Vol_i = (Wt_i/\rho_i)/ (\Sigma Wt_j/\rho_j) * 100\%$, where ρ_j are the mass densities of the crystalline phases calculated from the results of Rietveld refinement. *Wt* and their e.s.d.s are obtained by quantitative Rietveld refinement.
[d] Measured at 7 T and 2 K.
[e] Bimodal particle size distribution, see Figure S1 of SI.

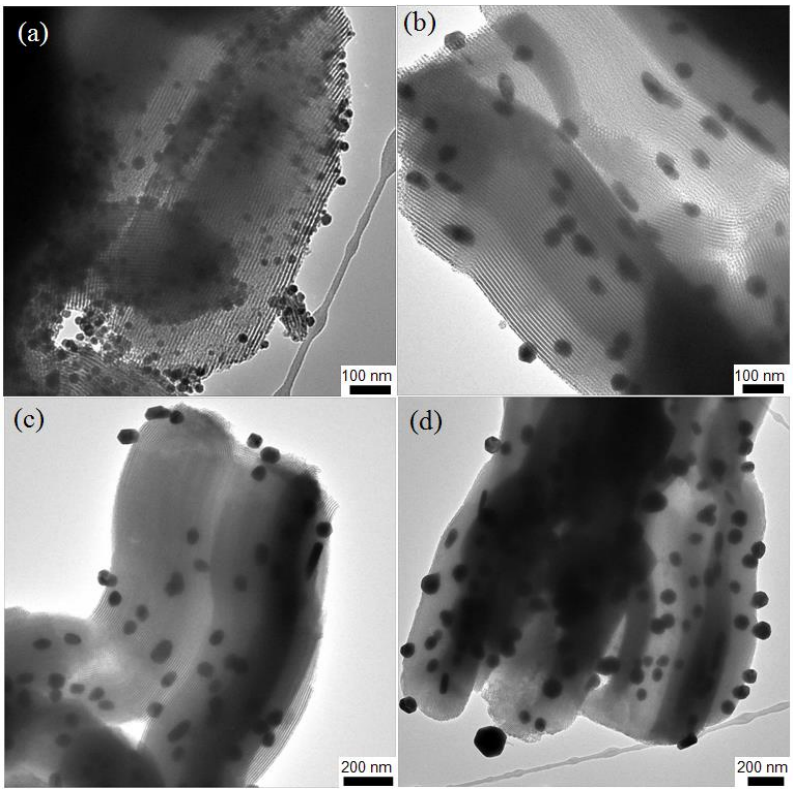

Figure 1. TEM micrographs of the SBA-15-supported Co-Ni-Ga nanoparticles with particle sizes of (a) 16 ± 5 nm and (b) 44 ± 10 nm for sample S30 with a bimodal particle size distribution (average particle size of 30 ±12 nm), (c) 68 ± 11 nm(sample S68), and (d) 84 ± 22 nm (sample S84).

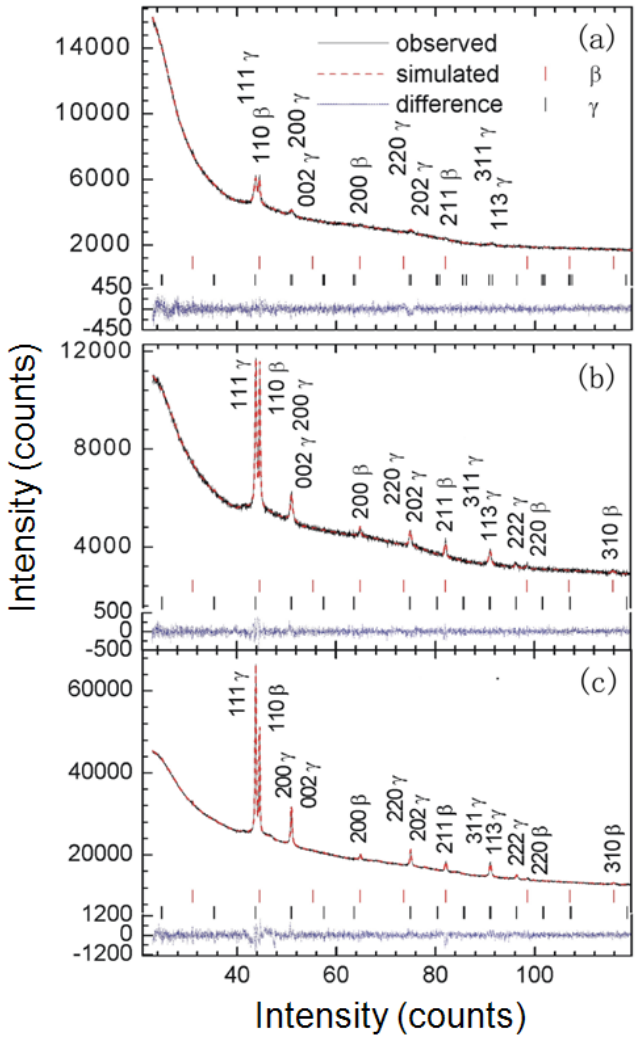

Figure 2. Experimental and Rietveld-simulated XRD patterns of Co-Ni-Ga nanoparticles with average particle sizes of (a) 30 nm (S30), (b) 68 nm (S68), and (c) 84 nm (S84).The reflection Miller indices *hkl* correspond to those of the cubic (β, ICSD #169729) and tetragonal (γ, ICSD #157778) crystalline phases of Co-Ni-Ga.

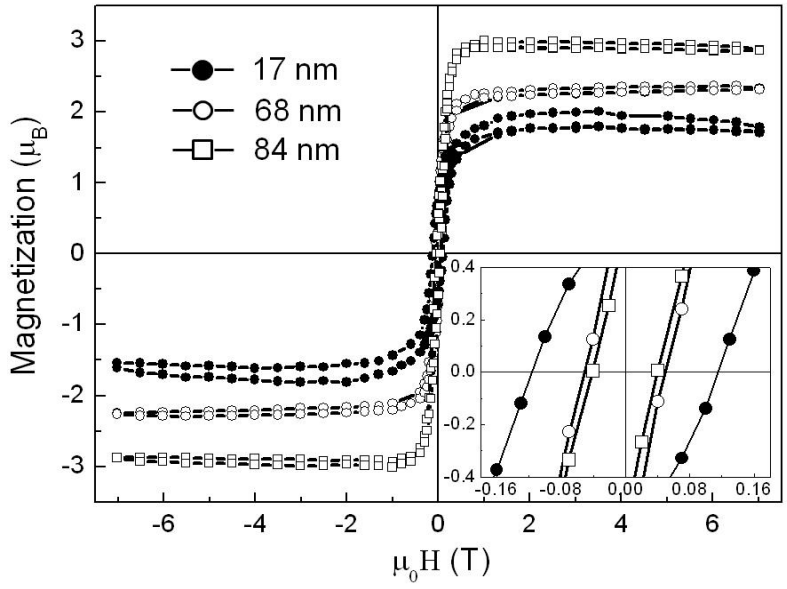

Figure 3. The field-dependent magnetization curves of Co-Ni-Ga nanoparticles of various sizes (S30, S68, and S84) measured at 2 K. The measured coercivity of the Co-Ni-Ga nanoparticles is shown in the inset, which magnifies the low-field portions.

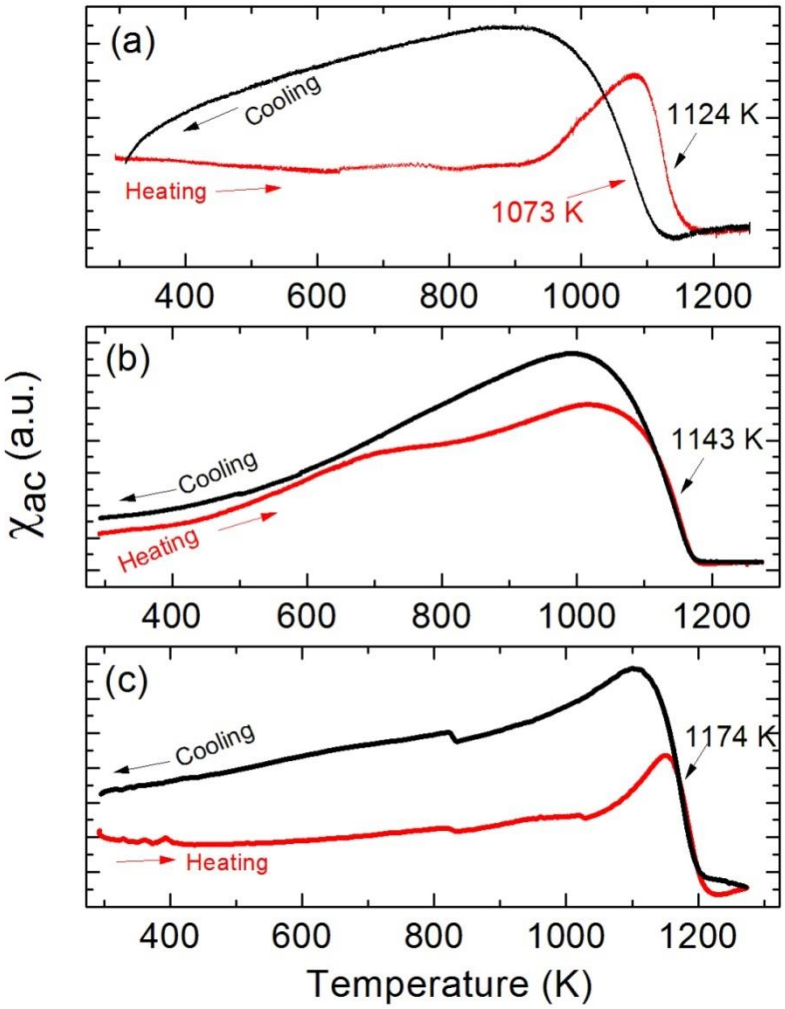

Figure 4. Thermomagnetic AC susceptibility profiles of Co-Ni-Ga nanoparticles (a) S30, (b) S68 and (c) S84. The derived Curie temperatures are indicated.

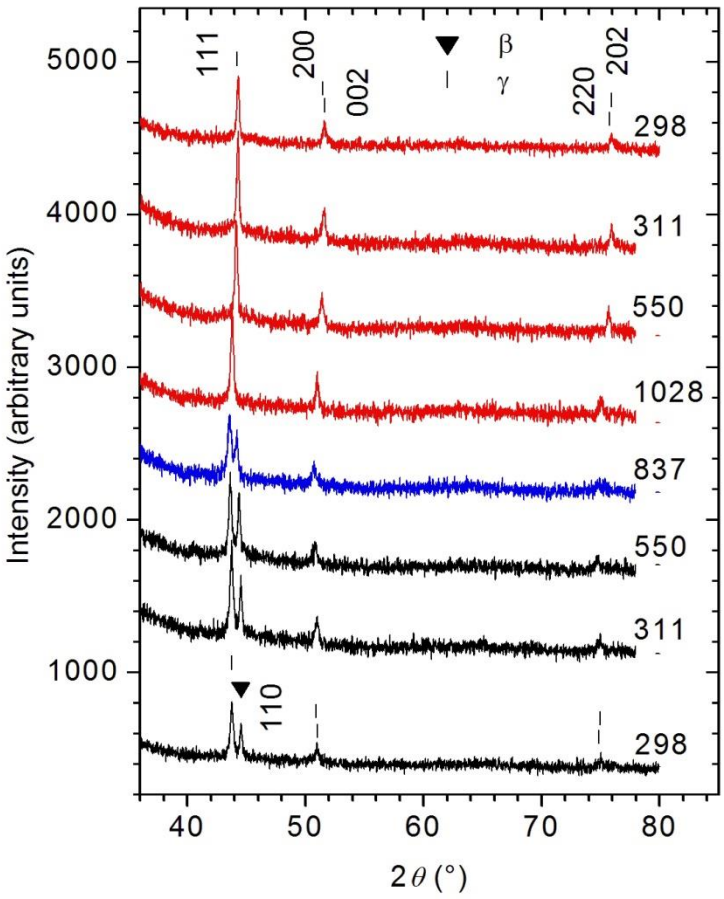

Figure 5. HT XRD patterns for Co-Ni-Ga nanoparticles sample S84. The temperatures of the measurement (in K) are shown in a right column of the Figure. For better comparison, the XRD patterns are shifted vertically from 298 K pattern (bottom) to 1028 K diagram in heating procedure and further to 298 K pattern (top) in cooling cycle. The Miller indices *hkl* of the observed reflections of the ß and γ phases are given.